International Journal of Innovative Computing, Information and Control
Volume **16**, Number **6**, December **2020**

ICIC International ©2020 ISSN 1349-4198
pp. **2007–2019**

CRACKS IN BRIDGE FLOOR DETECTED BY 2-DIMENSIONAL COMPLEX DISCRETE WAVELET PACKET TRANSFORM

Zhong Zhang[1], Ohzora Hamata[2], Takuma Akiduki[2], Tomoaki Mashimo[2]
Taiki Saito[3] and Kazuhiro Hayashi[3]

[1]Department of Intelligent Mechanical Engineering
Hiroshima Institute of Technology
2-1-1 Miyake, Saeki-ku, Hiroshima 731-5193, Japan
t.sho.g4@it-hiroshima.ac.jp

[2]Department of Mechanical Engineering
[3]Department of Architecture and Civil Engineering
Toyohashi University of Technology
1-1 Hibarigaoka Tenpaku-cho, Toyohashi 441-8580, Japan
{ akiduki; mashimo }@is.me.tut.ac.jp; tsaito@ace.tut.ac.jp

Received June 2020; revised October 2020

Abstract. *Bridge inspection is usually done visually on-site, and for this reason is problematic in places inaccessible to inspectors. In this paper we propose a solution through the analysis of features in captured images that suggest potential problems. We focus on the ability to detect cracks, and a complex-valued Haar wavelet is designed and applied to a 2D-CWPT, which is then combined with an anisotropic diffusion filter. A detection method for linear cracks is proposed through interpolation of the crack loss area and extraction processing according to the shape feature. The main results are: 1) we confirm that the complex-valued Haar wavelet is more effective for edge enhancement than the complex-valued Meyer wavelet; 2) quantitative evaluation of the proposed method for crack detection using the correct rate, sensitivity, specificity, precision rate, and F-value confirms the effectiveness of the method.*
Keywords: 2D-CWPT, Complex-valued Haar wavelet, Feature extraction, Crack, Frequency analysis, Image processing

1. **Introduction.** In the inspection of pillars and bridge floors, visual observation of cracks and confirmation of the state of the structure is considered to be an extremely important starting point for maintenance management. This is because the patterns and widths of cracks in concrete are closely related to deterioration. However, although it is easy to perform a direct visual inspection of concrete, other inspections have many elements that are based on the examiner's subjectivity and experience, and so an objective evaluation is difficult.

In recent years, however, the introduction of image processing technology for images from aerial photography and unmanned aerial vehicles has reduced both the production cost and the risk of human error, so that an optimization of objective and quantitative evaluations can be achieved. Further, image processing has been applied to surface inspection of concrete structures, such as pillars, and bridge floors, although there are still accuracy problems [1, 2, 3, 4]. These papers suggest methods to improve the performance of automatic detection of cracks from concrete surface images of pillars, bridge floors and so on.

DOI: 10.24507/ijicic.16.06.2007

The complex discrete wavelet packet transform (CWPT) is an alternative method used to improve the frequency resolution of the complex discrete wavelet transform (CDWT) [5]. An advantage of the CDWT is that the decomposition algorithm can be applied to high-frequency components, which contain a lot of information such as edges, and it is easy to extract information from locations where the brightness changes rapidly, such as at cracks. However, since the CWPT uses the complex-valued Meyer wavelet without compact support as a mother wavelet, edge extraction performance cannot be sufficiently achieved. The Haar wavelet, on the other hand, has compact support and is adaptable to edge extraction. However, the Haar wavelet has the disadvantage of being a real-valued wavelet without shift invariance and the extraction effect differs depending on the edge position.

In this study, we first design a complex-valued Haar wavelet and adapt it as the mother wavelet to the 2D-CWPT. We then apply it to the image processing of the 2D-CWPT. The resulting detection of any crack will verify its effectiveness. The remainder of the paper is organized as follows. In Section 2, the principle of the 2D-CWPT is introduced; in Section 3 the complex-valued Haar wavelet is designed and its characteristics are presented; in Section 4, the results of some experiments are given, and the performance of our method is graded. Finally, Section 5 contains some conclusions and closing remarks.

2. **Review of the Two-Dimensional Complex Wavelet Packet Transform (2D-CWPT).** The complex discrete wavelet transform (CDWT) is compatible with the conventional discrete wavelet transform (DWT), with the additional property that the signal can be completely reconstructed by using high-speed processing and conversion, or inverse transformations [6, 7]. It is characterized by a mother wavelet (MW), and is constituted by two orthogonal wavelets with real and imaginary parts. In this state, the scaling function has a real $\phi^R(x)$ and an imaginary $\phi^I(x)$ part. The MW similarly has a real $\psi^R(x)$ and an imaginary $\psi^I(x)$ part. In the time domain, the positions of the real and imaginary parts are shifted 1/2 sample towards each other, and this produces the conditions for shift invariance in the complex wavelet.

The CWPT is a method of producing improved frequency resolution of the CDWT [5]. The 2D-CWPT is a two-dimensional extension of the CWPT [8]. The 2D-CWPT, therefore, makes it possible to analyze detailed frequency components, unlike the conventional 2D-CDWT. Further, to increase the improvement and detection direction of the image resolution, the image needs to be broken down into fine frequency components. This can be done using the highly-accurate direction selectivity of the 2D-CWPT.

The 2D-CDWT, as well as the 2D-CWPT, can analyze a two-dimensional signal using the scaling function and the MW with the real and imaginary parts. However, the 2D-CWPT does not distinguish between wavelet coefficients of the high-frequency component and scaling coefficients of the low-frequency component, and therefore, all of the coefficients are recursively filtered by the 2D-CWPT. Moreover, each wavelet packet coefficient obtained by the 2D-CWPT in each analysis level (frequency band) is classified by the index (n, m) as is shown in Figure 1, where, Figure 1(a) shows decomposition level $j = -1$, and Figure 1(b) shows decomposition level $j = -2$. In the figure, n represents the vertical direction of the frequency component ω_y, and m represents the horizontal direction of the frequency component ω_x. If n and m are small numbers, they represent a low-frequency component. On the contrary, if n and m are large numbers, they represent a high-frequency component. Further, the analysis level $j = 0$ index $(1, 1)$ of the wavelet packet coefficient is expressed as $d^{(1,1)}_{0,k_x,k_y}$. It is equal to the scaling coefficient c_{0,k_x,k_y} of the conventional CDWT, and is given by Equation (1).

$$d_{0,k_x,k_y}^{(1,1)} = c_{0,k_x,k_y}, \tag{1}$$

where k_x and k_y show the position coordinates of the wavelet coefficient corresponding to the horizontal frequency ω_x and the vertical frequency ω_y, respectively. In addition, the wavelet packet coefficients vary in accordance with the analytical level and index.

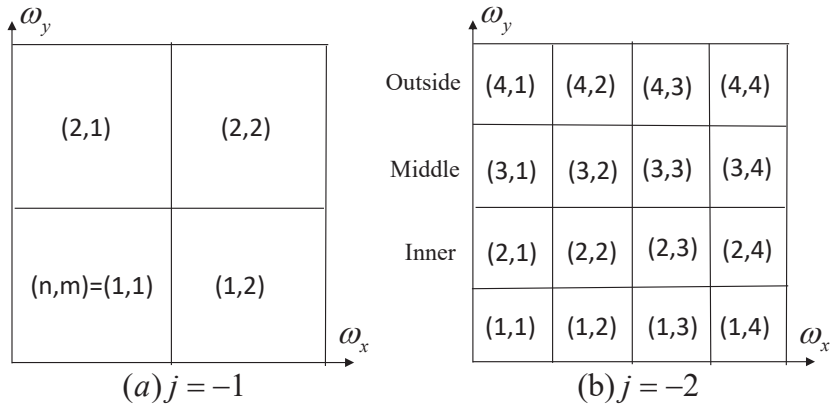

FIGURE 1. (color online) The index of each frequency component

In the image of the concrete, the background part is mainly included in the low-frequency components, and the cracked part is included in the relatively high-frequency components [10]. In this study, therefore, the 2D-CWPT decomposes the input image into level $j = -2$ to obtain the wavelet coefficients shown in Figure 1(b), where all the frequency components are divided into three major areas, in which the components of the region of $\max(n, m) = 2$ are defined as the low-frequency components (orange color), the components of the region of $\max(n, m) = 3$ are defined as the intermediate-frequency components (blue color), and the components of the region of $\max(n, m) = 4$ are defined as the high-frequency components (pink color).

The three major areas of frequency components are reconstructed to obtain three images respectively with different frequency features, and the result is shown in Figure 2, where, Figure 2(a) shows the original image, Figure 2(b) shows the image reconstructed by the low-frequency components with $\max(n, m) = 2$, Figure 2(c) shows the image reconstructed

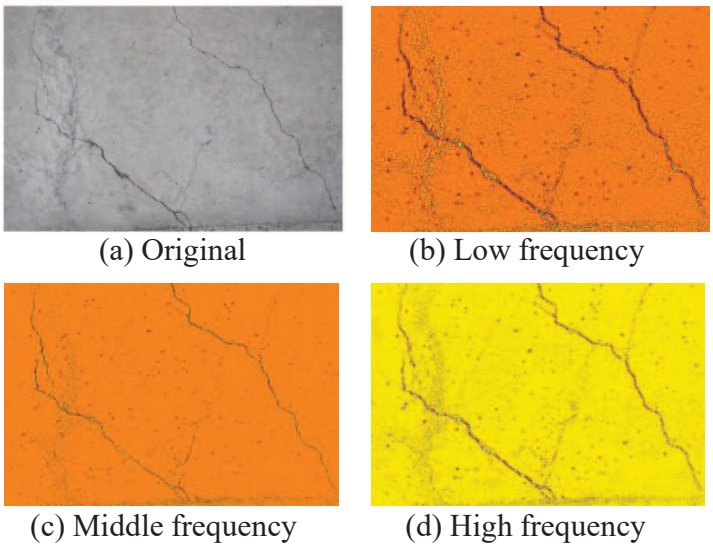

FIGURE 2. Example of three reconstructed images with different frequency components

by the intermediate-frequency components with $\max(n, m) = 3$ and Figure 2(d) shows the image reconstructed by the high-frequency components with $\max(n, m) = 4$. Comparing Figures 2(a), 2(b) and 2(c), it can be seen that the different frequency components were decomposed successfully.

3. Complex-Valued Haar Wavelet Design and Its Characteristics.

3.1. Complex-valued Haar wavelet design.

In the calculation of the 2D-CWPT, the MW ψ and the scaling function ϕ are not directly used, although the two-scale sequences p_k and q_k are used. In this section, therefore, the creation of the two-scale sequences is described in order. A detailed design method can be found in [7].

Generally, the Haar wavelet is a real-valued wavelet, and its two-scale sequence is expressed by the following equation [9].

$$p_k^R = 2^{1/2}(\delta_{0,k} + \delta_{1,k}), \tag{2}$$

where k shows number of the two-scale sequence p_k^R. The two-scale sequence of the imaginary part p_k^I can then be derived by using the following Equation (3) and Equation (4).

$$p_k^I = \sum_k p_k^R h_{n-2}, \tag{3}$$

$$h_n = \frac{1}{2\pi}\int_{-\pi}^{\pi} e^{i(n-1/2)\omega} d\omega = \frac{\sin(n - 1/2\pi)}{2 - 1/2\pi}. \tag{4}$$

It is possible to satisfy Equation (5) if the two-scale sequences p_k^R, p_k^I are properly designed.

$$\sum_k p_k = 2. \tag{5}$$

Further, the two-scale sequences q_k^R, q_k^I can be obtained from Equation (6) by using the two-scale sequences p_k^R, p_k^I.

$$q_k = (-1)^{1-k} p_{1-k}. \tag{6}$$

Figure 3 shows an example of the two-scale sequences of the designed complex-valued Haar wavelet, where Figure 3(a) shows the original Haar two-scale sequences p_k^R that were obtained by Equation (2), Figure 3(b) shows the two-scale sequences q_k^R that were obtained by Equation (6) using p_k^R, Figure 3(c) shows the two-scale sequences p_k^I that were obtained by Equations (3) and (4) using p_k^R, and Figure 3(d) shows the two-scale sequences q_k^I that were obtained by Equation (6) using p_k^I. Comparing the real and imaginary two-scale sequences p_k^R, p_k^I shown in Figures 3(a) and 3(c), it can be confirmed that the real part p_k^R has symmetry and imaginary part p_k^I has antisymmetry. Furthermore, it also can be confirmed that the symmetry centers of the real and imaginary parts deviate by 1/2 by the two-scale sequences p_k^R, p_k^I. Therefore, we can conclude that the designed complex-valued Haar wavelet is successful.

3.2. Achieved 2D-CWPT by using complex-valued Haar wavelet.

Since h_n shown in Equation (4) usually has an infinite length, the imaginary part of the two-scale sequence p_k^I obtained from the convolution of h_n and p_k^R by using Equation (3) also has an infinite length. However, only the two-scale sequence with finite length can be used for 2D-CWPT calculations, so the two-scale sequence p_k^I with infinite length must be truncated to become finite.

However, in the case of complex-valued Haar wavelets, the designed imaginary part has infinite length, so it is cut to a finite length to create a scaling function, and the result of performing an interpolation does not obtain satisfactory accuracy. In this study, therefore,

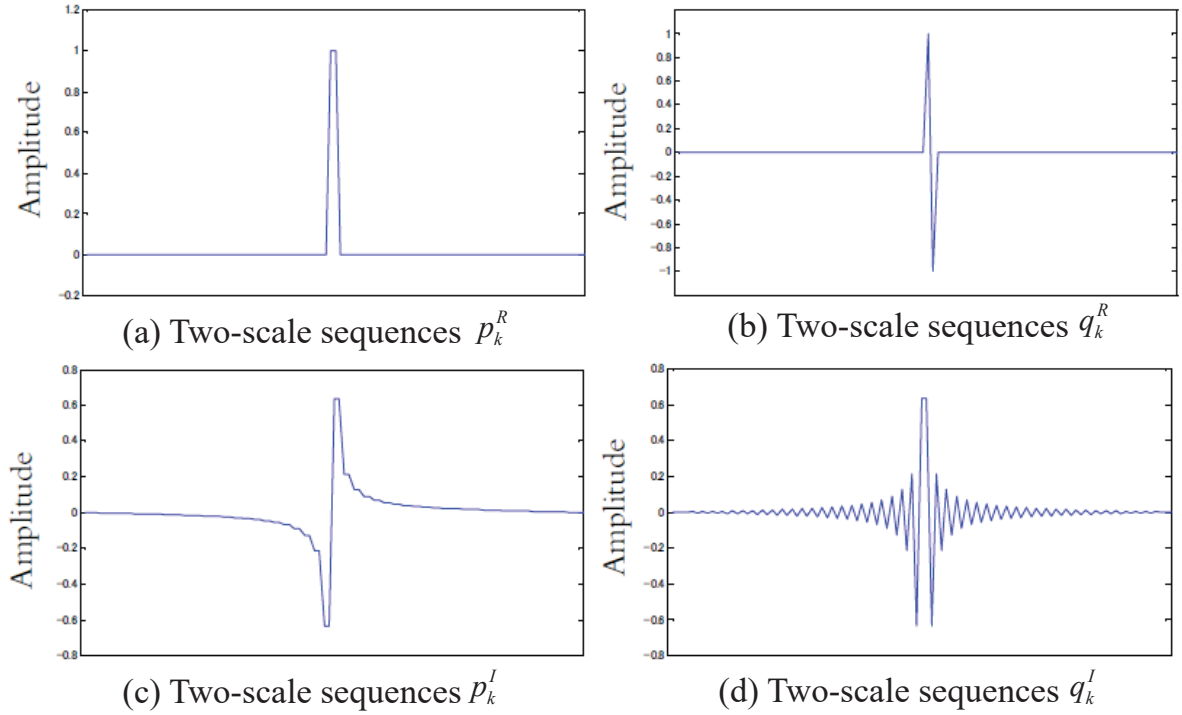

FIGURE 3. Designed complex-valued Haar wavelet two-scale sequences p_k^I, q_k^I from p_k^R by using Equations (3), (4) and (6)

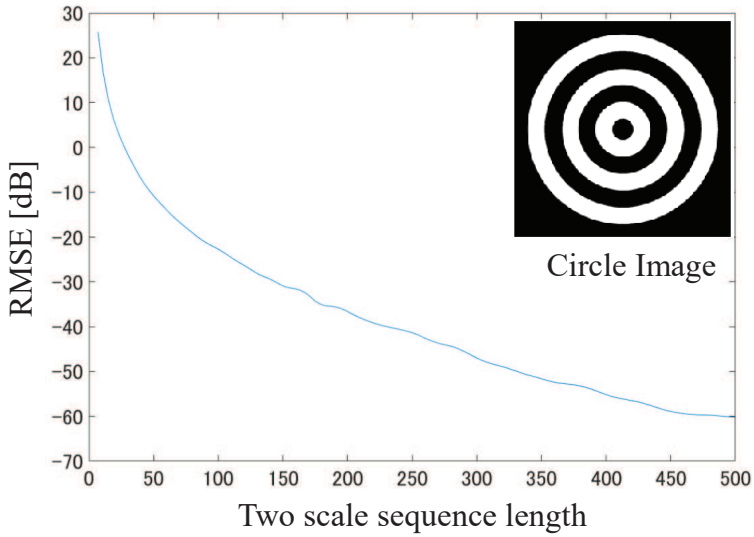

FIGURE 4. Influence of the two-scale sequence length of the imaginary part

to avoid the influence of interpolation on the calculation accuracy of 2D-CWPT, it was decided to use the scaling function of the Meyer wavelet [7] for interpolation calculation.

Figure 4 shows the influence of the two-scale sequence length of the imaginary part on the reconstruction accuracy of the circle model image. The circle image $f(x, y)$ shown in Figure 4 was firstly decomposed to level $j = -3$ by using the 2D-CDWT, and then reconstructed to form the original image $f'(x, y)$. The calculation error occurring in the decomposition processing and reconstruction processing was evaluated by using the root

mean squared error (RMSE) that is shown in the following equation:

$$\mathrm{RMSE} = 20\log_{10}\sqrt{\frac{1}{2}\sum\left(f(x,y) - f'(x,y)\right)^2} \quad [\mathrm{dB}]. \tag{7}$$

It can be seen from Figure 4 that the RMSE increases as the two-scale sequence length decreases, and when the length decreases around 220, the RMSE reaches -40 [dB], and when the length decreases below 100, the RMSE increases sharply. RMSE $= -40$ [dB] means that the average error of reconstruction is 1%, which almost satisfies the analysis accuracy in this study. In addition, the reconstruction accuracy of 2D-CDWT is RMSE $= -46.5960$ [dB] when the two-scale sequence length is 227, and in the 2D-CWPT used for crack detection, there is sufficient reconstruction accuracy up to level $j = -2$. Therefore, the two-scale sequence length of 227 has been selected in this study.

Figure 5 shows the edge detection results by the 2D-CWPT when the complex-valued Haar wavelet and complex-valued Meyer wavelet were used, where Figure 5(a) shows the model image, Figure 5(b) shows the edge detection results with the complex-valued Haar wavelet and Figure 5(c) shows the edge detection results with the complex-valued Meyer wavelet. In Figure 5, the high- and low-frequency components of the model image are reconstructed, respectively. As can be seen by comparing Figures 5(b) and 5(c), for the high-frequency and low-frequency components, the complex-valued Haar wavelet extracts the edge components better than the complex-valued Meyer wavelet does.

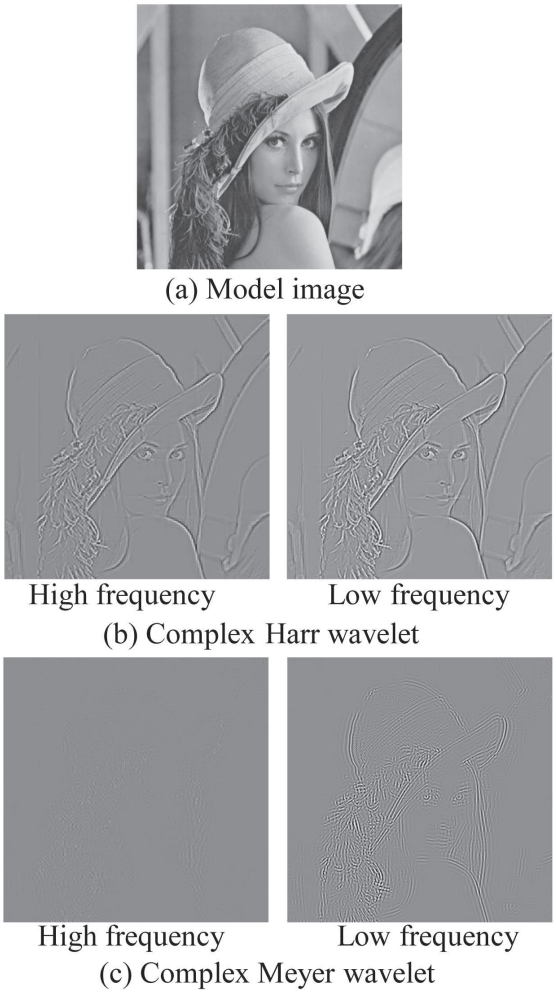

FIGURE 5. Example of edge detection using 2D-CWPT

4. Crack Detection in the Bridge Floor.

4.1. Crack detection process.

To achieve a robust crack extraction method from crack images by using image processing, 15 sample images taken under various conditions shown in Table 1 were selected by an expert. These 15 samples can almost be divided into four typical types, that is, 1) fine cracks on a non-uniform surface, 2) surface cracks including fine dirt, 3) exposed concrete and 4) moderate cracks on non-uniform surfaces. Furthermore, as can be seen from Table 1, the image size, brightness, the surface condition of the concrete, the condition of the cracks, etc. were quite different. In this study, the 15 sample images were used to confirm the proposed crack extraction method.

Table 1. Sample information

Sample No.	Image size	Brightness ave.	Image features
sample 1	1080×1920	0.690	Fine cracks on a non-uniform surface
sample 2	1080×1920	0.697	Fine cracks on a non-uniform surface
sample 3	1080×1920	0.690	Fine cracks on a non-uniform surface
sample 4	1014×2010	0.597	Uniform surface cracks (fine, medium)
sample 5	1170×3002	0.696	Exposed concrete
sample 6	1914×3342	0.603	Surface cracks including fine dirt (fine, medium)
sample 7	800×1200	0.668	Surface cracks containing some dirt (fine, medium)
sample 8	800×1200	0.701	Surface cracks containing some dirt (fine, medium)
sample 9	800×1200	0.667	Surface cracks containing some dirt (fine, medium)
sample 10	1968×2624	0.663	Surface cracks containing some dirt (repair, medium)
sample 11	1824×2736	0.613	Exposed concrete (with repairs)
sample 12	1824×2736	0.602	Exposed concrete (with repairs)
sample 13	1824×2736	0.469	Moderate cracks on non-uniform surfaces
sample 14	1824×2736	0.515	Moderate cracks on non-uniform surfaces
sample 15	1824×2736	0.490	Face cracks including fine dirt (fine, medium)

The flowchart of our proposed method is shown in Figure 6. Here, firstly as pre-processing, a color image was converted to gray scale, and padding processing performed. Next, the pre-processed image was decomposed into level $j = -2$ by the 2D-CWPT. After white noise was eliminated using wavelet thresholding (soft thresholding), three images with high-frequency, intermediate frequency and low-frequency components as shown in Figure 2 were reconstructed respectively. Binarization processing was then performed to separate the crack and the background. Since there are isolated points and missing areas in the binarized image, it was necessary to interpolate them. An interpolation processing was performed using the method combining an anisotropic diffusion filter and a distance image transformation proposed by Shirai et al. [11]. After interpolation processing, noise components other than the removal of isolated points were smoothed and became an elliptical object. Extraction processing was then performed with a reference eccentricity of 0.97 for the low-frequency image and 0.96 for the high-frequency image. Finally, the three images were combined into one image and output as the crack extraction result.

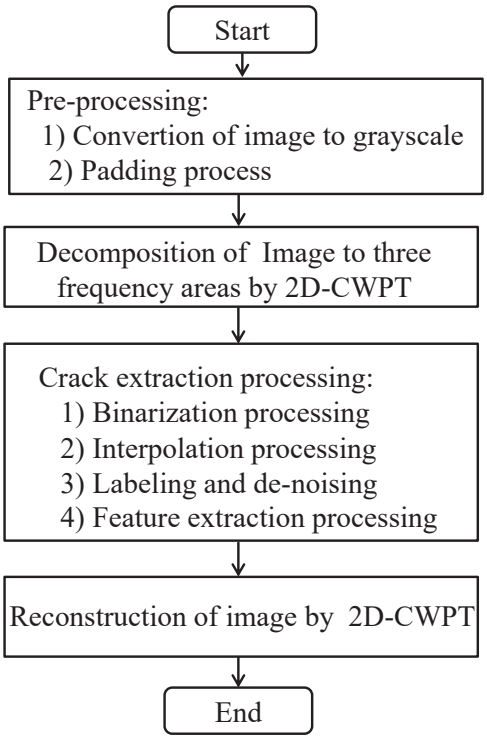

FIGURE 6. Flowchart for crack detection by using the 2D-CWPT

4.2. **Evaluation method of crack detection.** In this study, in order to evaluate the effectiveness of the proposed method, by following [12], the five indicators correct rate, sensitivity, specificity, precision rate and F-value were used. In order to compare with the proposed method, the binarization results of the representative discriminant analysis method by Otsu [13] were also evaluated by using the same method. Binarization is a particularly important step in the automatic extraction of cracks, and Otsu's method has the characteristic that the threshold value for binarization can be automatically selected when the histogram of the image shows bimodality.

First, the confusion matrix shown in Table 2 that summarizes the correctness of the class classification was made, where TP, FN, FP, and TN are abbreviations for true positive, false negative, false positive, and true negative, respectively. And each pixel of the image was classified into them. Then, for the 15 samples shown in Table 1, the indices correct rate, sensitivity, specificity, precision rate, F-value were calculated by the following Equations (8) to (12), where the index correct rate shows the correct rate of all the samples, the sensitivity shows the correct rate of the crack, the specificity shows the correct rate of the background, the precision rate shows the fitting degree of the crack, and the F-value shows the harmonic mean of the sensitivity and precision rate.

$$\text{Correct rate} = \frac{\text{TP} + \text{TN}}{\text{TP} + \text{TN} + \text{FP} + \text{FN}}, \tag{8}$$

$$\text{Sensitivity} = \frac{\text{TP}}{\text{TP} + \text{FN}}, \tag{9}$$

$$\text{Specificity} = \frac{\text{TN}}{\text{TN} + \text{FP}}, \tag{10}$$

$$\text{Precision rate} = \frac{\text{TP}}{\text{TP} + \text{FP}}, \tag{11}$$

$$F\text{-value} = \frac{2 \times \text{Sensitivity} \times \text{Precision rate}}{\text{Sensitivity} + \text{Precision rate}}. \tag{12}$$

TABLE 2. Confusion matrix

Original Date\Results	With Crack	No Crack
With Crack	TP	FN
No Crack	FP	TN

4.3. **Crack detected results and discussion.** The analysis results of sample 2, sample 8, and sample 13 are shown in Figures 7, 8, and 9, where, sample 2 is an example of fine

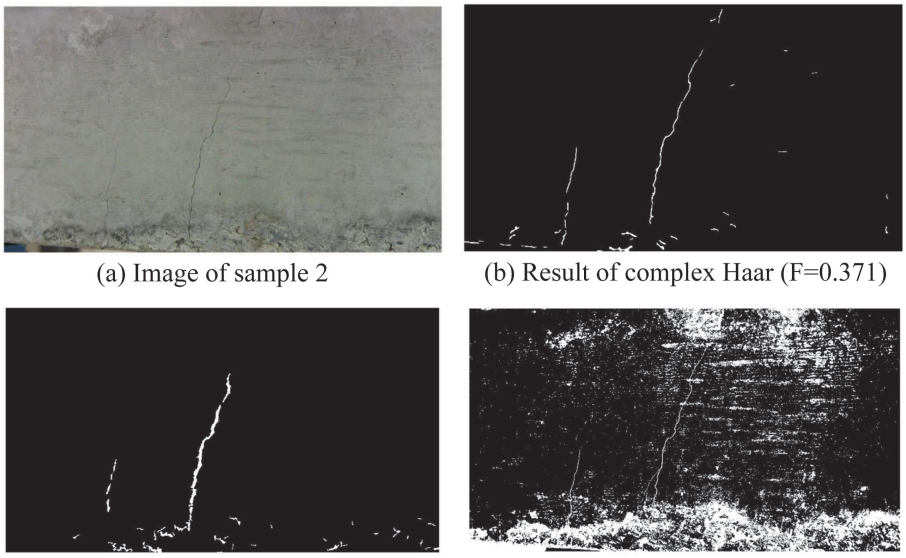

(a) Image of sample 2 (b) Result of complex Haar (F=0.371)

(c) Result of complex Meyer (F=0.201) (d) Result by Otsu's method (F=0.019)

FIGURE 7. Detection result from sample 2

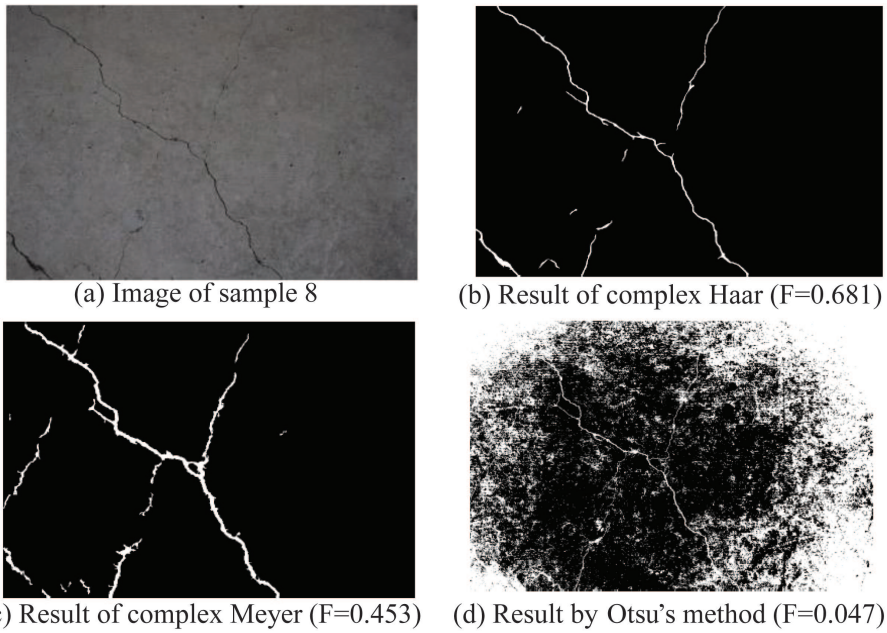

(a) Image of sample 8 (b) Result of complex Haar (F=0.681)

(c) Result of complex Meyer (F=0.453) (d) Result by Otsu's method (F=0.047)

FIGURE 8. Detection result from sample 8

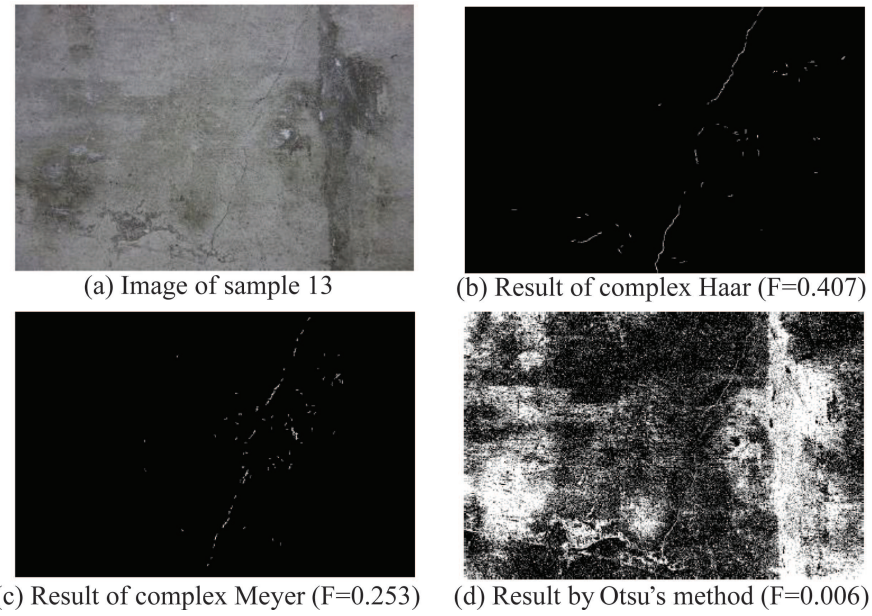

FIGURE 9. Detection result from sample 13

TABLE 3. Averaged analysis results of 15 samples

	Complex-valued Haar wavelet	Complex-valued Meyer wavelet	Otsu's method
Correct rate	0.996	0.990	0.654
Sensitivity	0.524	0.509	0.863
Specificity	0.998	0.992	0.653
Precision rate	0.534	0.247	0.073
F-value	0.506	0.297	0.076

cracks on a non-uniform surface, sample 8 is an example of a surface crack containing some dirt (fine, medium), and sample 13 is an example of moderate cracks on non-uniform surfaces. And in the figures, (a) shows the original image, (b) shows the crack detection results obtained by the complex-valued Haar wavelet, (c) shows the crack detection results obtained by the complex-valued Meyer wavelet and (d) shows the crack detection results obtained by Otsu's method. Further, the averaged values of the 15 samples for the indices correct rate, sensitivity, specificity, precision rate and F-value are shown in Table 3.

Looking at Figures 7, 8, and 9 firstly, the cracks are detected more clearly using the complex-valued Meyer wavelet than using the complex-valued Haar wavelet. However, the width of the detected cracks was wider than the original width of the cracks. Further, when the detected cracks were enlarged, it can be seen that interference fringes were also generated. In contrast, the crack width was detected more accurately using the complex-valued Haar wavelet. Then focusing on the precision rate and F-value, for the samples shown in Figures 7, 8 and 9, the values of the evaluation index by the complex-valued Haar wavelet were higher than those by the complex-valued Meyer wavelet. It was evaluated that the crack detection capability of the complex-valued Haar wavelet was relatively high.

On the other hand, when we examine the results focusing on the sensitivity shown in Table 3, the change of the index in Otsu's method is remarkable. However, according to the results of Otsu's method, the sensitivity is extremely high and the precision rate

is extremely low, so that the F-value, which is the harmonic mean of the two indices, decreases. It is considered that this is due to the high sensitivity and sensitive reaction to changes in brightness other than cracks, resulting in excessive crack detection. Therefore, in crack detection, the complex-valued Haar wavelet is better when evaluated from the F-value, and it is considered that the purpose of this study was achieved.

Further, looking at the averaged values of the 15 samples for all the indices shown in Table 3, the complex-valued Haar wavelet values are higher than those of the complex-valued Meyer wavelet and Otsu's method, and higher-specificity results were found. From these results, it can be said that the proposed method is effective for crack detection.

However, there are exceptions depending on the sample. It is sample 12 in which cracks exist on the surface of the exposed concrete including the repair marks shown in Figure 10. Otsu's method cannot accurately extract cracks because this sample has local brightness changes such as surface unevenness noise and repair marks. On the other hand, the complex-valued Meyer wavelet has the best results. It can be seen from the five indices shown in Table 3 that the detection result of the complex-valued Haar wavelet was superior to that of Meyer so far in most images. However, in this type of sample, the complex-valued Meyer wavelet has an F-value of about 0.2 higher than that of the complex-valued Haar wavelet, and it also can be judged that the detection result of the complex-valued Meyer wavelet was excellent in the qualitative evaluation by visual observation.

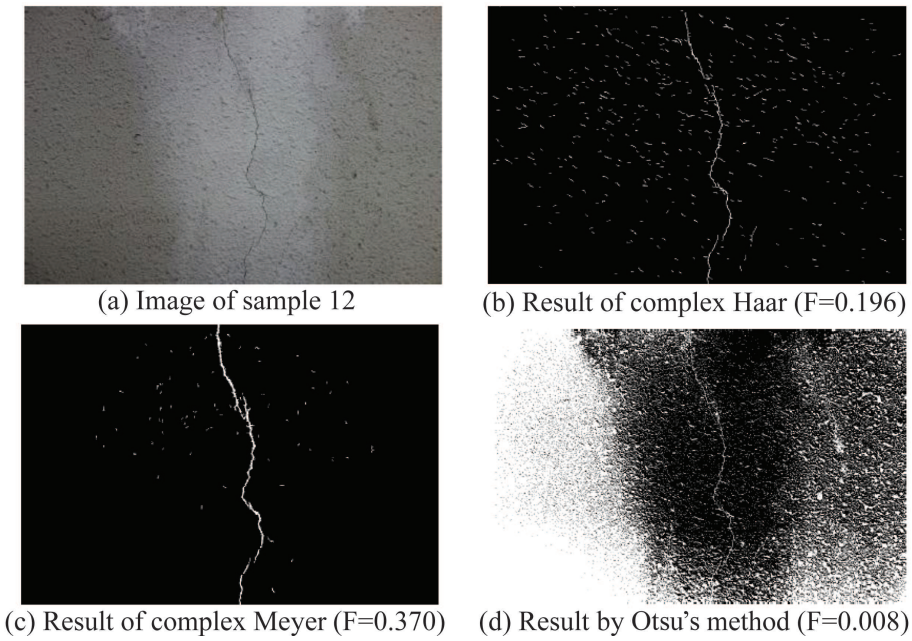

FIGURE 10. Detection result from sample 12

There are several possible causes for this, but it is mainly due to the amount of noise present in the sample image. In the detection result of the complex-valued Haar wavelet, many noises on the surface irregularities remain even after the interpolation processing and the extraction processing. On the other hand, the detection result of the complex-valued Meyer wavelet is less affected by noise than the complex-valued Haar wavelet, and only the edges of major cracks were extracted. The difference in this result is considered to be in the binarization threshold. The binarization has a strong threshold dependency, and in this study the threshold was set by using the characteristics of the time-frequency image, but it was shown that it could not be applied to samples with extremely noisy data.

From this, it was confirmed that the method of determining the threshold considering the characteristics of the input image is an important issue in the future of this research.

5. **Conclusion and Remarks.** In this study, we focused on the ability to detect cracks, and designed a complex-valued Haar wavelet, and applied it to the 2D-CWPT. The 2D-CWPT and anisotropic diffusion filter were combined and tested, and a crack detection method for linear cracks was proposed through interpolation of the crack loss area and extraction processing according to the shape feature. The results obtained are as follows.

1) We designed a complex-valued Haar wavelet and applied it to 2D-CWPT image processing. The results confirmed that the complex-valued Haar wavelet is more effective for edge enhancement than the complex-valued Meyer wavelet.
2) Focusing on the 2D-CWPT that can analyze detail in time-frequency analysis, we proposed a method to separate an image into three partial images according to frequency characteristics. This made it possible to perform analysis focusing on global frequency components.
3) The proposed method was evaluated quantitatively using measurement for correct rate, sensitivity, specificity, precision rate, and F-value that are often found in similar studies [12]. The result confirmed that the proposed method using the complex-valued Haar is effective for crack detection.

There are many noises on the surface of exposed concrete. For such a surface, a method of determining the threshold value considering the characteristics of the input image is an important issue for our future research.

Acknowledgment. This work was partially supported by JSPS KAKENHI Grant Numbers 16H03143 and 19H02223. The authors also gratefully acknowledge the helpful comments and suggestions of the reviewers.

REFERENCES

[1] T. C. Hutchinson and Z. Q. Chen, Improved image analysis for evaluating concrete damage, *Journal of Computing in Civil Engineering*, vol.20, no.3, pp.2010-2016, 2006.
[2] P. J. Chun, N. Kataoka, C. Miwa, K. Hashimoto and M. Ohga, Crack detection from an image of concrete surface with considering statistical and geometrical characteristics, *Journal of Japan Society of Civil Engineers F3 (Civil Informatics)*, vol.70, no.2, pp.1-8, 2014 (in Japanese).
[3] L. Zhang, F. Yang. Y. D. Zhang and Y. J. Zhu, Road crack detection using deep convolutional neural network, *Proc. of 2016 IEEE International Conference on Image Processing (ICIP2016)*, pp.3708-3712, 2016.
[4] L. Guo, R. Li, B. Jiang and X. Shen, Automatic crack distress classification from concrete surface images using a novel deep-width network architecture, *Neurocomputing*, vol.397, pp.383-392, 2020.
[5] H. Toda, Z. Zhang and T. Imamura, The design of complex wavelet packet transforms based on perfect translation invariance theorems, *International Journal of Wavelets, Multiresolution and Information Processing*, vol.8, no.4, pp.537-558, 2010.
[6] N. G. Kingsbury, The dual-tree complex wavelet transform: A new technique for shift invariance and directional filters, *IEEE Digital Signal Processing Workshop (DSP1998)*, pp.2543-2560, 1998.
[7] H. Toda and Z. Zhang, Perfect translation invariance with a wide range of shapes of Hilbert transform pairs of wavelet bases, *International Journal of Wavelets, Multiresolution and Information Processing*, vol.8, no.4, pp.501-520, 2010.
[8] T. Kato, Z. Zhang, H. Toda, T. Imamura and T. Miyake, A novel design method for directional selection based on 2-dimensional complex wavelet packet transform, *International Journal of Wavelets, Multiresolution and Information Processing*, vol.11, no.4, 2013.
[9] A.-H. Najmi, *Wavelets: A Concise Guide*, The Johns Hopkins University Press, 2012.
[10] Z. Zhang, O. Hamada, H. Toda, T. Akiduki and T. Miyake, Bridge floor cracks detection by using the 2 dimensional complex discrete wavelet packet transform, *Proc. of the 2016 International Conference on Wavelet Analysis and Pattern Recognition (ICWAPR2016)*, pp.225-229, 2016.

[11] K. Shirai, A. Kitadai, S. Inoue et al., *Image Processing for Historical Character Shape Retrieval*, IPSJ SIG Technical Reports, vol.2013-CH-97, no.7, pp.1-6, 2013 (in Japanese with English abstract).
[12] Y. Fujita, H. Nakamura and Y. Hamamoto, Automatic and exact crack extraction from concrete surfaces using image processing techniques, *Journal of Japan Society of Civil Engineers*, vol.66, no.3, pp.459-470, 2010 (in Japanese with English abstract).
[13] N. Otsu, A threshold selection method from gray-level histograms, *IEEE Trans. Sys. Man. Cyber.*, vol.9, no.1, pp.62-66, 1979.